

GHGT-11

To a dynamic update of the Sleipner CO₂ storage geological model using 4D seismic data

Alexandre Fornel^{a,*} and Audrey Estublier^a

^a IFP Energies nouvelles, 1-4 avenue de Bois Préau, 92852 Rueil-Malmaison, France

Abstract

A new methodology has been developed for history matching seismic impedances from 3D reservoir fluid flow and petro-elastic simulations with those obtained by 4D (time-lapse) seismic inversion. The objective is to build predictive flow models directly constrained by the geological (borehole) and geophysical (seismic) information. To reduce differences between simulation and observation, an optimization process updates a set of chosen uncertain model parameters to at least obtain an optimal model that provides simulation results closer to the measured data. In the frame of the CO₂ReMoVe European project, this methodology was applied on the Utsira sand formation where CO₂ is stored at Sleipner.

© 2013 The Authors. Published by Elsevier Ltd.
Selection and/or peer-review under responsibility of GHGT

Keywords: Carbon geological storage; Sleipner; history matching; geological model; 4D seismic.

1. Introduction

According to different geological studies performed in the region around the Sleipner field [1,2,3], it is admitted that the Utsira sand formation is mainly composed of coarse sandstone and thin shale layers. In the storage area, covered by the 4D seismic, only two wells are present: the CO₂ injector and an old appraisal well. It is therefore difficult to precisely know the location and the extension of the shale beds except at wellbore. The first effect was that early CO₂ migration simulations were not at all able to mimic the observation. To mitigate with such a problem and on the basis of seismic interpretation, artificial chimneys were introduced in the model to be more efficient in CO₂ migration modeling. The locations of these artifacts were determined by analyzing the different 3D seismic performed on the Sleipner field. Although this approach allows the model to reproduce a CO₂ plume consistent with seismic observations,

* Corresponding author. Tel.: +33-147525723; fax: +33-147527046.
E-mail address: Alexandre.FORNEL@ifpen.fr.

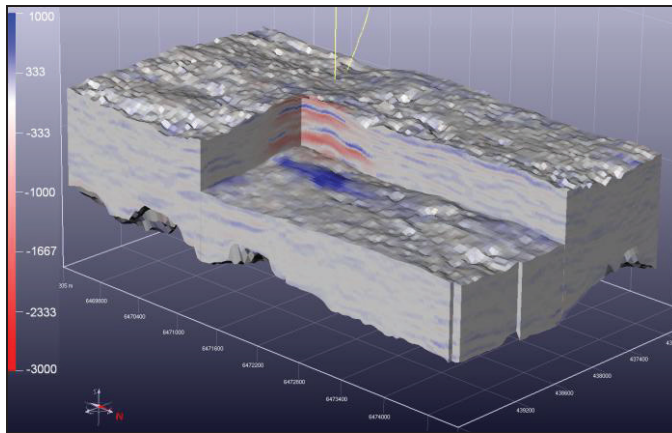


Fig. 2. Differences of P-wave elastic impedance between 1994 and 2006 seismic surveys (1994 vintage being acquired prior to CO₂ injection)

2.1. Construction of the geological facies model

To build a geological facies model consistent with observed data, our methodology is based on two main criteria [4]. At first, an analysis of the formula defining compressional and shear impedances shows that the relative variation of the bulk modulus between two seismic surveys can be expressed as a simple function [4,5] of the relative variation of the two types of impedances. Moreover, a significant variation of the incompressibility corresponds to a fluid substitution effect and, in our case, tells us about the substitution of the brine in place by CO₂. Thus, by combining impedances coming from the seismic inversion, we obtain reliable information on the CO₂ location in the reservoir and we can say that, in this specific area of our model, we have mainly sandstone facies. But this single criterion (noted C1) does not permit to locate the shale beds because of their low thickness (less than one meter in general). So a second criterion (noted C2) is introduced when making a lithologic classification based on the I_p/I_s ratio [5], usually higher in shales than in sandstones. This approach allows to delineate the base of the shale beds. Subsequently we denote:

- C1 = 1 if the relative variation of the bulk modulus is greater or equal to 15%;
- C2 = 1 is the second criterion identifies the base of a shale bed.

We have chosen to perform a facies geostatistical simulation with only two facies (sandstone and shale), using a non-stationary facies proportion derived from the interpretation of seismic information. But rather than working on facies proportions defined cell by cell, we focused on creating zones where the shale proportion is constant but used as a parameter of the history matching and will therefore be adjusted by the 4D seismic information. One advantage of this approach is to be able to vary the proportions in each zone independently. The optimization process adjusts these proportion and thus controls the occurrence and extension of shale barriers that will enable or not the migration of the CO₂.

2.2. Fluid flow modeling

The chosen values for sandstones porosity (37%) and horizontal permeability (3 darcys) represent mean values determined on core from the well 15/9-A23 [6]. The rock compressibility for each facies is derived from the study by Carcione [13]. In order to reduce computing time of fluid flow simulations,

grid blocks containing shale are defined as dead cells and the dissolution phenomenon is not taken into account in the fluid flow simulation performed in the history matching loop.

We consider an injection of pure CO₂ in a saline aquifer. A more complete study should consider that the injected gas is composed of 99% CO₂ and 1% CH₄. The water density and viscosity are computed from internal correlation models [7] based on pressure, temperature and salinity. The Peng-Robinson equation of state is used to calculate the gas density and the Lohrenz-Bray-Clark [8] one for the gas viscosity.

2.3. Petro-elastic modeling

The saturation-pressure patterns obtained from the fluid flow simulation are mapped onto compressional velocities and impedances at each cell. A number of quantitative relationships have been published in the public literature to link elastic properties of rocks with their pore space, densities, fluid saturation, pore pressure and rock composition [9], many of these relationships are based on empirical correlations. Other relationships derive from effective medium theory and hence are subject to different types of operating assumptions [10,11,12].

The petro-elastic model is based on Gassmann's equations [9,10] which calculates velocities and impedances for P- and S-waves as a function of saturations, pressures and densities of fluids in place, and some petro-elastic parameters such as bulk and shear moduli. The model is completed by Hertz-Mindlin's equations [13,14] which take into account the effects of pressure changes on seismic velocities.

The next key step in our technique is the depth-time conversion. Using seismic velocity cubes given by the petro-elastic model, we are able to transform impedance cubes from the depth domain to the time domain. The main advantage is to build a velocity law cell by cell and to update it during the optimization process and through time. Therefore we always have travel times coherent with impedances (often, only a constant seismic velocity cube is used for the entire optimization and for the different seismic surveys, or only averaged velocities between seismic markers).

The obtained impedances are then filtered in the bandwidth of the seismic data (the same as the one used in the seismic inversion). It remains then to calculate the differences of impedance between the base and different available seismic surveys: here, we are only using 1994 and 2006 surveys. Improvement would be to consider successively all the vintages to consolidate our model over time while reducing uncertainties.

2.4. Objective function: least squares criterion

The update of the geological model by the dynamic data depends on the minimization of an objective function that measures the mismatch between the observed data (production and 4D seismic-related data) and the obtained simulation results for a fixed value of the parameters θ . The least-squares formulation is frequently used in the oil industry:

$$J(\theta) = \frac{1}{2} (S^{obs} - S(\theta))^T C_s^{-1} (S^{obs} - S(\theta))$$

where S^{obs} is the 4D seismic-related data, $S(\theta)$ is the simulated seismic results for the parameter value θ , and C_s is the covariance matrix on the seismic data. This matrix represents the uncertainty on

the residual between measured and simulated data. Errors are assumed independent in our case, therefore the covariance matrix is diagonal.

The minimization of the objective function requires the calculation of the derivatives of the simulation results with respect to the parameters to estimate:

$$\frac{\partial S}{\partial \theta} \theta$$

In this study, a finite-difference approximation is used for the calculation of the derivative of the simulation results with respect to the parameterization of the fine-scale geostatistical model. This choice allows a quick application of our 4D workflow without requiring any additional programming in the fluid flow simulator or the petro-elastic modeling.

2.5. Optimization techniques

The algorithms of non-linear optimization calculate, a value θ^{opt} of the parameters, according to an iterative process which minimizes the objective function. An iteration of the optimization algorithm determines an estimate of the parameters according to this principle:

$$\theta^{k+1} = \theta^k + t^k s^k$$

The direction s^k is the solution of a particular linearized problem. The formulation of this problem depends upon the simulation results as well as their derivative with respect to the parameterization.

The step t^k is calculated to satisfy the descend relation:

$$J \theta^k + t^k s^k < J \theta^k$$

Various methods of optimization, such as the steepest descent, Fletcher–Powell, Levenberg–Marquardt and the Gauss–Newton, are implemented. In this study, we choose to work with the Fletcher–Powell algorithm, which offers the advantages of both the steepest-descent (stability and robustness far from the solution) and Gauss–Newton methods (fast convergence in the neighborhood of the solution). A general overview of optimization methods has been given by Lions [15].

3. Optimization results

3.1. Initial geological model

The general principle was previously described: the key point of this methodology is to build zones combining the two criteria detailed in Section 2.1 and to assign an initial vertical shale proportion to each zone based on geological and seismic data. Four zoning approaches have been established, each step benefiting from results of the previous one. Here we only present the final step.

We define three zones (Table 1) to better propagate parameters changes in the entire model. The first zone Z1 contains all gridblocks where the sandstone facies is potentially dominant: the initial shale proportion is set to 0.1. The second zone Z2 characterizes gridblocks where the dominant facies is probably shale but where the presence of some gas can also be deduced from the seismic interpretation: the initial shale proportion is thus set to 0.5. The last zone Z3 corresponds to gridblocks verifying C2=1 (i.e. potentially shale), C1=0 (i.e. no presence of CO₂) and for which the cell immediately below verifies

C1=1 (i.e. presence of CO₂). These gridblocks correspond potentially to shale and form a barrier to the CO₂ migration: therefore, we are likely in presence of shale and we attribute an initial shale proportion equal to 1.

Table 1. Zones definition for the geomodel of the last step of the optimization process.

Zone name	C1 criterion	C2 criterion	Initial shale proportion Psh
Zone Z1	0 or 1	0	0.1
Zone Z2	1	1	0.75
Zone Z3	0	1	1

For this optimization we choose to vary the following parameters (Table 2): the correlation length in X-direction (Lx) and Y-direction (Ly), the shale proportions in zones Z1 (Psh_Z1) and Z2 (Psh_Z2).

Table 2. Initial values and variation range of parameters for the last optimization.

Parameter	Initial value	Minimal value	Maximal value
Lx (m)	500	250	750
Ly (m)	500	250	750
Psh_Z1	0.1	0.01	0.25
Psh_Z2	0.75	0.5	1.

3.2. Objective function evolution

The final step of the optimization process stopped after 13 simulations for which the objective function values are illustrated in Fig. 3. Values are presented in percentage of the result obtained for the initial model (in green). In red, we have the value obtained for the optimal set of parameters and in purple values obtained for the intermediate simulations. We notice a strong decrease of the mismatch between simulation results and 4D seismic data (-25%).

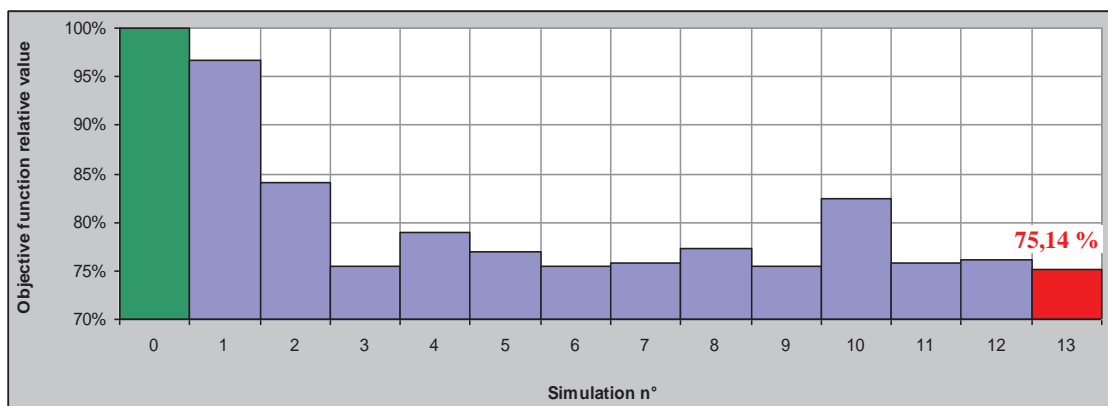


Fig. 3. Objective function evolution for the fourth step of the optimization process. In green the value obtained for the initial model; in red the one for the optimal model.

The analysis of optimal parameters values shows that the model needs more than 15% of shale in the sandstone zone and that the correlation lengths are slightly longer (525 m) than those defined for the initial model. The optimized facies model is shown in Fig. 4 (b). We remark an improvement of the lateral continuity of facies proportions and the stratification of shale layers is very well depicted, this denotes a better geological consistency.

3.3. Seismic impedance variations and saturation

When observing results for CO₂ saturations shown in Fig. 4, we denote a trend to the expected "Christmas tree" shape of the CO₂ plume with a large amount of CO₂ trapped between the intermediate shale beds reflecting a better consistency with 4D seismic data.

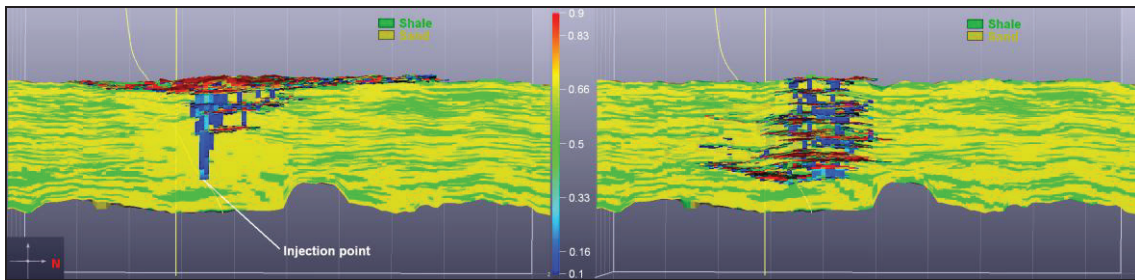


Fig. 4. CO₂ saturation in 2006 - 2D East view: (a) with initial model ; (b) with optimal model

The results may be still improved in terms of differences of simulated impedances: the variation range is globally underestimated and the optimization algorithm has difficulties to reproduce observed variations outside the plume. Such a behavior suggests that the least squares formulation is perhaps not the most appropriate for matching seismic attributes. It would be interesting to test the impact of a new formulation of the objective function developed by IFPEN [16] which is based more on the geometry of 4D anomalies and is particularly adapted to the problem we meet here.

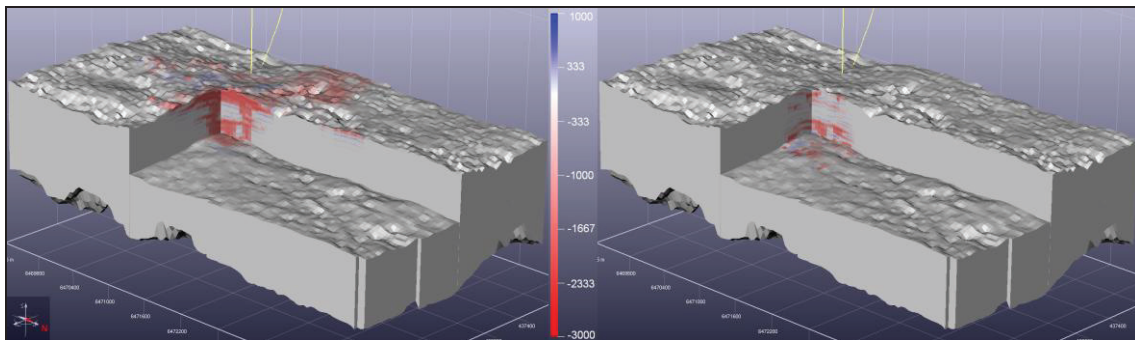


Fig. 5. (a) Initial $\Delta I_p(2006-1994)$; (b) Optimal $\Delta I_p(2006-1994)$.

4. Conclusion

We have applied a new methodology for history matching of 4D seismic data to Sleipner CO₂ storage data. A massive use of previous works done both in geophysics and geology allowed us to build an initial

facies model consistent with observations. Then, the methodology aims at constraining quantitatively this initial model with the inverted 4D seismic data and leads to a model entirely consistent with geophysics, geology and fluid flow.

Various tests of zoning coupled to the optimization of facies proportions in each area finally lead to a model compatible with the geological facies and providing fluid flow results fairly close to what is observed on different seismic images. It is important to note that the optimal model still needs to be further improved, but it has already the advantage of being not constrained artificially and should thus provides higher predictability. The methodology would be more efficient if using more wells to elaborate the initial geomodel and integrating all the time lapse surveys (including shear impedances) in the processing.

Acknowledgements

The authors thank the CO2ReMoVe European project (Contract n° SES6 518350 funded by the EU 6th framework program and industry partners BP, ConocoPhillips, ExxonMobil, Statoil, Schlumberger, Total, Vattenfall and Wintershall) to allow the publication of this work. They are also grateful to all partners for fruitful technical comments during project discussion. The success of the CO2ReMoVe project depends to a large degree on the accessibility of the storage sites and associated data, we thank Statoil for their strong collaboration.

References

- [1] Isaken D, Tonstad K. A revised Cretaceous and Tertiary lithostratigraphic nomenclature for the Norwegian North Sea. NPD Bulletin 5, Oljedirektoratet; 1989.
- [2] Wilkinson IP. The biostratigraphical and palaeo-ecological application of calcareous microfaunas from the Utsira Formation in Norwegian well 15/9-A-23. BGS Technical Report WH99/124R; 1999.
- [3] Piasecki S, Gregersen U, Johannessen PN. Lower Pliocene dinoflagellate cysts from cored Utsira Formation in the Viking Graben, northern North Sea. *Marine and Petroleum Geology* 19; 2002, p. 55-67.
- [4] Clochard V, Delépine N, Labat K and Ricarte P. CO2 plume imaging using 3D pre-stack stratigraphic inversion: A case study on the Sleipner field, *First Break*, 28 (1), 91–96, 2010.
- [5] Dubos-Sallée N, Rasolofosaon P. Data-driven quantitative analysis of the CO2 plume extension from 4D seismic monitoring in Sleipner. 72nd EAGE Conference & Exhibition incorporating SPE EUROPEC 2010, Barcelona, Spain., Paper K010; 2010.
- [6] Pearce JM, Kemp SJ, Wetton PD. Mineralogical and Petrographical Characterization of 1m core from the Utsira formation, Central North Sea. *British Geological Survey, Report WG/99/24C*; 1999, p. 26.
- [7] Schmidt E. *Properties of Water and Steam in SI Units*. Springer Verlag; 1969.
- [8] Lohrenz J, Bray B, Clark C. Calculating Viscosities of Reservoir Fluids from Compositions. *Journal of Petroleum Technology*; Oct. 1964
- [9] Mavko G, Mukerji T, Dvorkin J. *The Rock Physics Handbook: Tools for Seismic Analysis in Porous Media*. Cambridge University Press, United Kingdom; 1998
- [10] Gassmann F. Über Die Elastizität Poröser Medien. *Vierteljahresschrift Naturforschungs Gesellschaft*, vol. 96, Zurich, Switzerland; 1951, p. 1-23.
- [11] Ramamoorthy R, Murphy WF, Coll C. Total porosity estimation in shaly sands from shear modulus. *Proceedings of SPWLA 36th Annual Logging Symposium Transactions*; 1995.
- [12] Rasolofosaon P, Zinszner B. Petroacoustic characterization of reservoir rocks for seismic monitoring studies. Laboratory measurement of Hertz and Gassmann parameters. *Oil & Gas Science Technology*, vol. 58, n°6; 2003, p. 615-635.
- [13] Carcione JM, Picotti S, Gei D, Rossi G. Physics and Seismic Modeling for Monitoring CO2 Storage. *Pure and Applied Geophysics* 163; 2006, p. 175-207.
- [14] Zweigel P, Heill LK. Studies on the likelihood for caprock fracturing in the Sleipner CO2 injection case – a contribution to the Saline Aquifer CO2 Storage (SACS) project. *SINTEF Petroleum Research Report*, 33.5324.00/02/03; 2003, p. 27.
- [15] Lions JL. *Contrôle optimal de systèmes gouvernés par des équations aux dérivées partielles*. Dunod; 1968.
- [16] Patent EP 11.290.122.8. 2011.